Liquid Crystals
Publication details, including instructions for authors and subscription information:
http://www.informaworld.com/smpp/title~content=t713926090

Synthesis and characterisation of main-chain hydrogen-bonded supramolecular liquid crystalline complexes formed by azo-containing compounds

Cher Ling Toh[ab]; Jianwei Xu[a]; Xuehong Lu[b]; Chaobin He[a]
[a] Institute of Materials Research and Engineering, Singapore 117602, Singapore [b] School of Materials Science and Engineering, Nanyang Technological University, Singapore 639798, Singapore

To cite this Article Toh, Cher Ling , Xu, Jianwei , Lu, Xuehong and He, Chaobin(2008) 'Synthesis and characterisation of main-chain hydrogen-bonded supramolecular liquid crystalline complexes formed by azo-containing compounds', Liquid Crystals, 35: 3, 241 — 251
To link to this Article: DOI: 10.1080/02678290701862355
URL: http://dx.doi.org/10.1080/02678290701862355

Liquid Crystals,
Vol. 35, No. 3, March 2008, 241–251

Taylor & Francis
Taylor & Francis Group

Synthesis and characterisation of main-chain hydrogen-bonded supramolecular liquid crystalline complexes formed by azo-containing compounds

Cher Ling Toh[ab], Jianwei Xu[a]*, Xuehong Lu[b] and Chaobin He[a]*

[a]*Institute of Materials Research and Engineering, 3 Research Link, Singapore 117602, Singapore;* [b]*School of Materials Science and Engineering, Nanyang Technological University, Nanyang Avenue, Singapore 639798, Singapore*

(Received 29 January 2007; in final form 26 November 2007)

A series of azopyridine-containing hydrogen bonding acceptors (**4a**–**c**) with flexible spacers of oligo(methylene) were synthesised. Hydrogen-bonded polymeric complexes **4/5** and trimeric complexes **4/6$_2$**, where **5** and **6** are aromatic dicarboxylic acids and monocarboxylic acids, respectively, were prepared and their liquid crystallinity was examined using differential scanning calorimetry and polarising optical microscopy. The study showed that most of the complexes displayed reversible thermotropic nematic phase. The isotropic to nematic phase transition temperatures of polymeric complexes **4/5** and trimeric complexes **4/6$_2$** in general decreased with the increase in length of spacers and terminal groups in the corresponding proton acceptors **4** and the proton donors **5** and **6**, respectively. Hydrogen bonding interactions in complexes **4/5** and **4/6$_2$** were studied by X-ray photoelectron spectroscopy and Fourier transform infrared spectroscopy.

Keywords: azo compounds; hydrogen bonding; liquid crystals; synthesis

1. Introduction

Non-covalent interactions, particularly hydrogen bonding (H-bonding), have been demonstrated to be powerful for inducing various types of supramolecular structures. Much work has been directed towards the synthesis and development of liquid-crystalline polymeric structures (*1–3*). For example, main-chain linear hydrogen-bonded (H-bonded) liquid crystals (LCs) formed by bipyridyl derivatives and aromatic dicarboxylic acids were widely investigated by Griffin et al. (*4–8*). Lee et al. (*9*) reported that polyoxyethylene-spacered bis(biphenyl) dicarboxylic acid and 4,4′-bipyridine formed hexagonal columnar and bicontinuous cubic LCs. Main-chain thermotropic or lyotropic LCs formed by triple H-bonding complementary molecules were also reported by Lehn (*10, 11*). Recently, we reported on flexible chain-spacered stilbazole derivatives which formed polymeric supramolecular main-chain thermotropic LCs (*12, 13*). It is of interest to study whether analogous azo-containing compounds can form similar supramolecular polymeric LCs. Aromatic azo-containing compounds (Ar–N=N–Ar′) can undergo a much easier photo-induced *trans–cis* isomerisation than C=C and thus can form more interesting photoactive LCs. Among these photoactive mesogenic units, azobenzene derivatives are most extensively investigated. The rigid rod-like structure of azobenzene molecules makes them suitable candidates for exhibiting liquid crystallinity (*14, 15*). On the other hand, the unique characteristics of azobenzene molecules provides the possibility of molecular motion in response to light or heat and thus offer many opportunities in photonic applications. In such azo-containing liquid crystalline materials, the azo-containing moiety is usually incorporated into the side chain of the polymer backbone to induce the formation of LCs (*16–21*). Alternatively, azopyridine units could act as H-bonding donors in a side chain to generate H-bonded supramolecular LCs (*22, 23*). Azopyridine-containing compounds has also been demonstrated to form H-bonded dimeric liquid crystalline complexes (*24*). However, there had been limited reports on main-chain LC systems that include azo-containing compounds (*25, 26*). Thus, in an effort to explore whether difunctional azo-containing compounds form polymeric LCs, this article provides an insight into the synthesis and properties of azo-containing H-bonded main-chain supramolecular polymers. In order to enhance the understanding of such azopyridine compounds, trimeric complexes with mono-substituted benzoic acids are also examined. The H-bonding interactions in both polymeric and trimeric complexes are investigated by X-ray photoelectron spectroscopy (XPS) and Fourier transform infrared spectroscopy (FT-IR). The thermal properties of the liquid crystalline complexes were examined using differential scanning calorimetry (DSC) and polarising optical microscopy (POM).

*Corresponding authors. Email: jw-xu@imre.a-star.edu.sg; cb-he@imre.a-star.edu.sg

ISSN 0267-8292 print/ISSN 1366-5855 online

DOI: 10.1080/02678290701862355
http://www.informaworld.com

2. Experimental details

2.1. *Methods*

The nuclear magnetic resonance (NMR) spectra were acquired on a Bruker DRX 400 MHz spectrometer in deuterated solvent with tetramethylsilane (TMS) as an internal standard. XPS measurements were carried out on a Kratos AXIS HSi spectrometer with a monochomatised Al Kα X-ray source (1486.71 eV photons). FT-IR spectra were measured on a Perkin-Elmer FT-IR spectrophotometer 2000 using KBr pellets. Mass spectra were determined on a VG Micromass 7035 mass spectrometer at 70 eV with electron impact ionisation (EI). Thermal behaviours of the H-bonded complexes were studied on a TA Instrument DSC 2920 under a heating and cooling rate of 5°C min^{-1} in nitrogen. The peak temperatures of the endotherms and exotherms were taken as the phase transition temperatures. The photomicrographs of the complexes were taken under a Nikon OPTIPHOT2-POL polarising optical microscope fitted with a hot stage using a temperature programmer TP-93 and a TMC-6RGB1/2″ colour CCD camera. The sample was placed on a glass slide, covered with a glass coverslip and heated on the hot stage at a rate of 10°C min^{-1} and cooled at 2°C min^{-1}. The UV spectra were measured on film samples prepared by spin coating onto quartz. The film samples were then dried in vacuum oven at room temperature to remove residual solvent before the spectra were recorded on a Shimadzu Model UV-2501PC UV-visible spectrophotometer. A Blak-Ray high-intensity lamp Model B-100AP (365 nm, 100 W) was used to induce photoisomerisation of the azo-containing compounds.

2.2. *Chemical reagents*

Compounds 4-hexyloxybenzoic acid (**6a**) and 4-dodecyloxybenzoic acid (**6d**) were purchased from Sigma-Aldrich. The dibenzoic acids **5a**–**c** were synthesised according to methods reported in the literature (*27*). Other chemical reagents were used as received.

2.3. *4-(4-Hydroxyphenylazo)pyridine (3)*

4-(4-Hydroxyphenylazo)pyridine (**3**) was synthesised according to methods reported in the literature (*23*). Yield: 43%. Melting point: 227°C. ^{1}H NMR (DMSO-d_6, 25°C, δ ppm): 11.01 (s, 1H), 8.96 (s, 2H), 8.04 (d, 2H, J=6.0 Hz), 7.95 (d, 2H, J=8.0 Hz), 7.04 (d, 2H, J=8.0 Hz).

2.4. *General synthetic procedures for 4a–c*

A mixture of **3** (5 mmol), alkyl dibromide (2.5 mmol) and anhydrous K_2CO_3 (0.77 g, 5.57 mmol) in dry N,N-dimethylformamide (DMF; 40 ml) was heated at 110–120°C in nitrogen for 3–5 h. The reaction mixture was cooled to room temperature and poured into ice water with stirring. The suspension was filtered and the residue was washed with water. The residue was re-dissolved in chloroform, then washed with water and dried with anhydrous $MgSO_4$. The drying agent was filtered off and the organic solvent was removed under reduced pressure. The residue was chromatographed on silica gel twice using chloroform/methanol as an eluent and further purified by preparative thin layer chromatography to afford compound **4** as a yellow solid.

2.5. *1,8-Bis{4-(pyridin-4-ylazo)-phenoxy}-octane (4a)*

Yield: 15%. Melting point: 174°C. FT-IR (KBr): 3042, 2951, 2917, 2869, 2855, 1603, 1582, 1500, 1470, 1453, 1417, 1323, 1297, 1259, 1141, 1028, 988, 841, 796, 559 cm^{-1}. ^{1}H NMR ($CDCl_3$, 25°C, δ ppm): 8.78 (s, 4H), 7.96 (d, 4H, J=8.8 Hz), 7.68 (d, 4H, J=3.2 Hz), 7.02 (d, 4H, J=8.8 Hz), 4.07 (t, 4H), 1.89–1.82 (m, 4H), 1.52–1.44 (m, 8H). ^{13}C NMR δ 162.91, 157.51, 151.21, 146.79, 125.64, 116.23, 114.92, 68.47, 29.29, 29.15, 25.97. MS (EI, *m*/*z*): 508.4 (M^+). Analysis for $C_{30}H_{32}N_6O_2$: calculated: C, 70.84; H, 6.34; N, 16.52; found: C, 70.46; H, 6.33; N, 16.06.

2.6. *1,10-Bis{4-(pyridin-4-ylazo)-phenoxy}-decane (4b)*

Yield: 12%. Melting point: 161°C. FT-IR (KBr): 3034, 2942, 2918, 2867, 2849, 1603, 1584, 1500, 1471, 1455, 1418, 1319, 1300, 1253, 1146, 1014, 842, 797, 558 cm^{-1}. ^{1}H NMR ($CDCl_3$, 25°C, δ ppm): 8.79 (s, 4H), 7.96 (d, 4H, J=8.92 Hz), 7.69 (s, 4H), 7.02 (d, 4H, J=8.92 Hz), 4.07 (t, 4H), 1.87–1.80 (m, 4H), 1.50–1.37 (m, 12H). ^{13}C NMR δ 162.93, 157.50, 151.18, 146.77, 125.62, 116.25, 114.91, 68.51, 29.47, 29.34, 29.15, 26.00. MS (EI, *m*/*z*): 536.2 (M^+). Analysis for $C_{32}H_{36}N_6O_2$: Calculated: C, 71.62; H, 6.76; N, 15.66; Found: C, 71.77; H, 6.82; N, 15.28.

2.7. *1,12-Bis{4-(pyridin-4-ylazo)-phenoxy}-dodecane (4c)*

Yield: 20%. Melting point: 153°C. FT-IR (KBr): 3049, 2945, 2918, 2850, 1604, 1584, 1501, 1471, 1455, 1419, 1319, 1299, 1256, 1145, 1032, 841, 796, 560 cm^{-1}. ^{1}H NMR ($CDCl_3$, 25°C, δ ppm): 8.80 (s, 4H), 7.96 (d, 4H, J=8.8 Hz), 7.70 (s, 4H), 7.02 (d, 4H, J=9.2 Hz), 4.06 (t, 4H), 1.87–1.80 (m, 4H), 1.51–1.32 (m, 16H). ^{13}C NMR δ 162.96,

157.53, 151.13, 146.78, 125.63, 116.28, 114.92, 68.55, 29.56, 29.37, 29.16, 26.01. MS (EI, *m/z*): 564.3 (M^+). Analysis for $C_{34}H_{40}N_6O_2$: Calculated: C, 72.31; H, 7.14; N, 14.88; Found: C, 71.95; H, 7.16; N, 14.39.

2.8. *General synthesis for 6b, c*

A mixture of methyl 4-hydroxybenzoate (5.0 g, 32.9 mmol), 1-bromooctane or 1-bromodecane (32.9 mmol), and anhydrous K_2CO_3 (4.77 g, 34.51 mmol) in 2-butanone (80 ml) was gently refluxed for 2 days. After the reaction was complete, the reaction mixture was cooled to room temperature and filtered. An oily liquid was collected after removal of the solvent from the filtrate under reduced pressure. The oily liquid was then refluxed with 200 ml of 10% potassium hydroxide (w/v) in 95% ethanol for 5 h. The excess ethanol was removed under reduced pressure and the residue was dissolved in water. The solution was then acidified with concentrated hydrochloric acid to pH=1. The resulting white precipitate was collected by filtration, dried and purified twice by re-crystallisation from ethanol to give compound **6** as a white solid.

4-Octyloxybenzoic acid **(6b)**: Yield: 45%. Melting point: 146°C. ^{1}H NMR (DMSO-d_6, 25°C, δ ppm): 7.87 (d, 2H, J=7.3 Hz), 7.00 (d, 2H, J=7.3 Hz), 4.03 (t, 2H), 1.75–1.69 (m, 2H), 1.41–1.39 (m, 2H), 1.29–1.26 (m, 8H), 0.86 (t, 3H). Analysis for $C_{15}H_{22}O_3$: Calculated: C, 71.97; H, 8.86. Found: C, 71.67; H, 8.99.

4-Decyloxybenzoic acid **(6c)**: Yield: 43%. Melting point: 141°C. ^{1}H NMR (DMSO-d_6, 25°C, δ ppm): 7.87 (d, 2H, J=8.7 Hz), 6.99 (d, 2H, J=8.8 Hz), 4.03 (t, 2H), 1.75–1.68 (m, 2H), 1.41–1.37 (m, 2H), 1.33–1.25 (m, 12H), 0.85 (t, 3H). Analysis for $C_{17}H_{26}O_3$: Calculated: C, 73.34; H, 9.41. Found: C, 73.17; H, 9.60.

2.9. *Formation of complexes*

All H-bonded complexes were prepared using the melt method. A stoichiometric mixture of a proton acceptor and a proton donor was heated in an oil bath at temperatures above their melting points with vigorous magnetic stirring. A 1:1 or 1:2 of a proton acceptor to a proton donor was used for polymeric complexes or for trimeric complexes, respectively. The mixtures were allowed to remain in their melt state for about 1 min before they were air-cooled to room temperature. The H-bonded complexes for composition study were prepared from a mixture of **4c**, **5b** and **6d** in different molar ratios.

3. Results and discussion

3.1. *Synthesis of monomers and complexes*

The synthetic route leading to compounds **4a**–**c** is shown in Scheme 1. First, 4-(4-hydroxyphenylazo)-pyridine **3** (see (*22*)) was prepared by adding phenol, sodium nitrite and sodium hydroxide aqueous solution dropwise into a mixture of 4-aminopyridine and hydrochloric acid solution at around 0°C. Compound **3** then reacted with suitable alkyl dibromides to afford compounds **4a**–**c**. The chemical structures of **4a**–**c** were characterised by spectroscopic methods and elemental analysis. For example, in the ^{1}H NMR spectrum of compound **4a**, two doublets at δ 7.96 and 7.02 with a coupling constant of J=8.8 Hz, corresponding to phenoxy protons, were observed. Seven aromatic carbon signals appeared in its ^{13}C NMR spectrum, indicating that the chemical structure of **4a** was consistent with our expectation. All monomers **4a**–**c** showed that the molecular ions in their EI mass spectra and their elemental analyses were in good agreement with the theoretical values. The polymeric complexes **4/5** and trimeric complexes **4/6$_2$** were prepared using the melt method as described in the experimental section and their molecular structures, proton donors as well as the molecular structures of reference polymeric complexes **7/5** are depicted in Scheme 2.

3.2. *XPS and FT-IR study*

The non-covalent H-bonding interaction between the acceptor and donor molecules was studied using XPS. It was reported that the binding energies of elements involving in the formation of H-bonding such as nitrogen and neighbouring carbon atoms are sensitive to the changes in the chemical environment. Thus, the shift in binding energy provides useful information on the type of interaction between donor and acceptor molecules (*28–32*). Complexation of the acceptor and donor molecules causes a delocalisation of electron charge. Subsequently, there is an induced

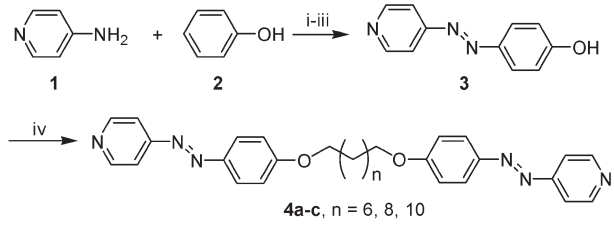

Scheme 1. The synthetic route of H-bond acceptors **4a**–**c**. Reagents and conditions: (i) HCl; (ii) $NaNO_2$, NaOH(aq), 0°C; (iii) adjust pH to 6–7 using NaOH(aq); (iv) $BrCH_2(CH_2)_nCH_2Br$ (n=6, 8, 10), K_2CO_3, DMF, 110–120°C, N_2.

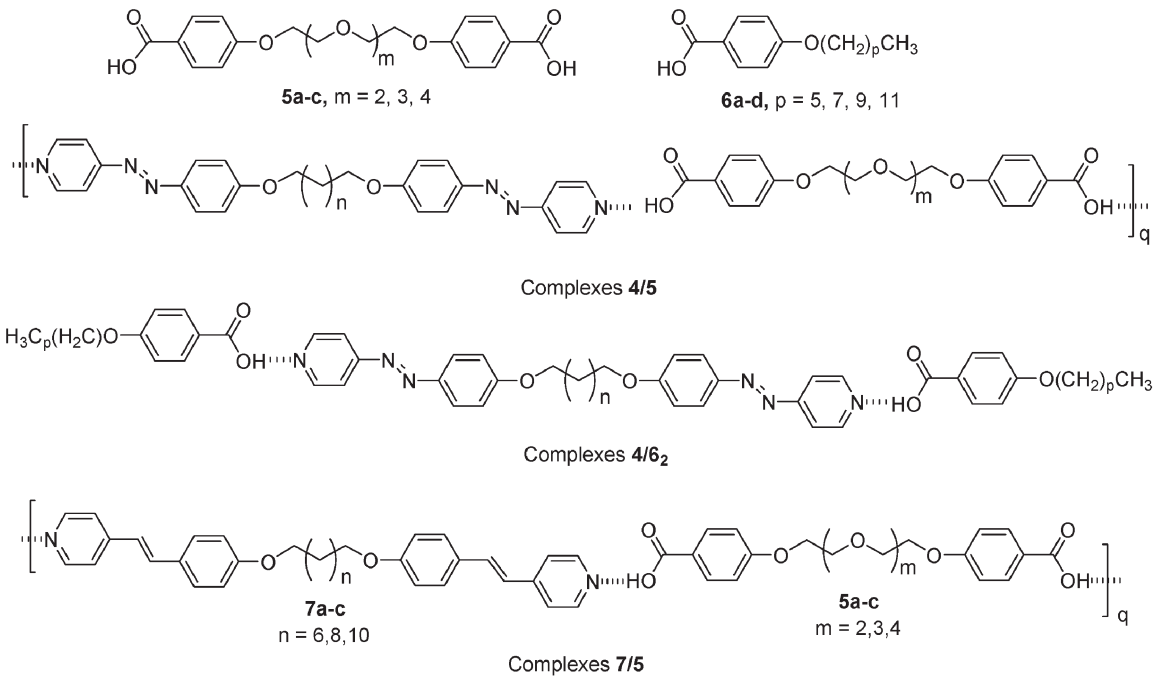

Scheme 2. The molecular structures of H-bond donors **5a–c** and **6a–d** and H-bonded complexes **4/5**, **4/6$_2$** and **7/5**.

change in electron density at the specific atoms, thus resulting in the shifts in binding energy. Moreover, the magnitude of shifts in binding energy could be used to determine the type of associated interaction in the complexes.

The XPS spectra for several selected complexes were determined and the N 1s and C 1s spectra of polymeric complexes **4a/5b**, **4b/5b** and **4c/5b**, as well as the acceptor **4b** and the donor **5b**, are shown in Figure 1. The spectra were deconvoluted by employing a combination of Gaussian (80%) and Lorentz (20%) methods. The binding energies of N 1s for pyridine and carbonyl C 1s are also summarised in Table 1. The N 1s spectrum of the uncomplexed

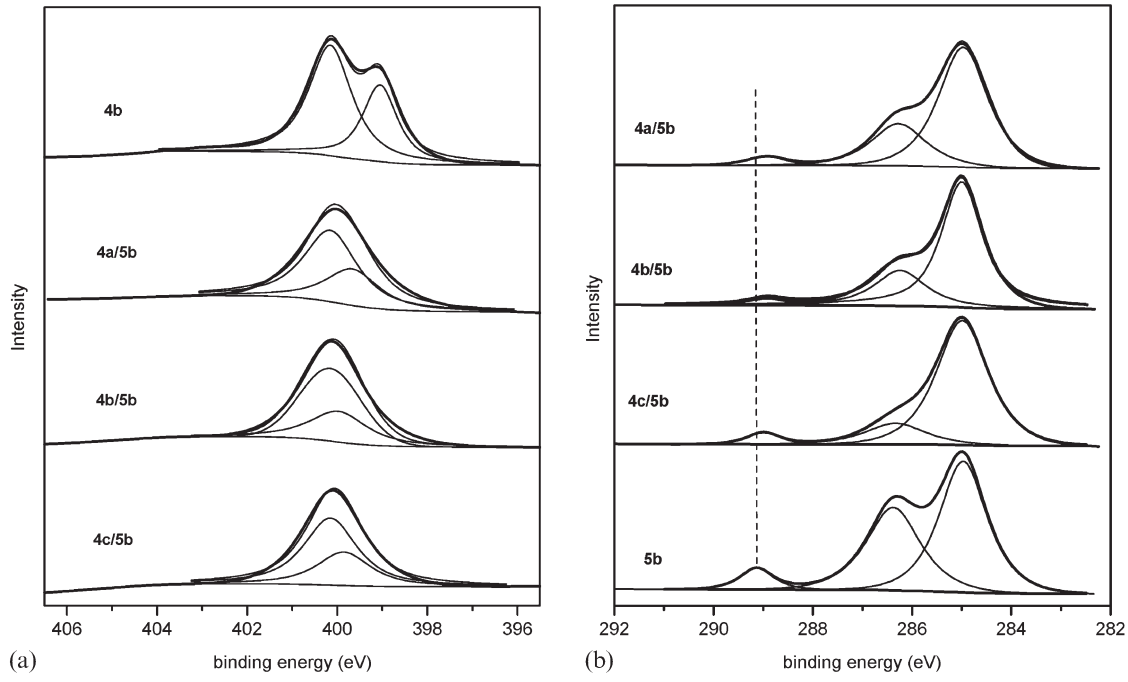

Figure 1. (a) N 1s spectra of **4b**, **4a/5b**, **4b/5b** and **4c/5b** and (b) C 1s spectra of **4a/5b**, **4b/5b**, **4c/5b** and **5b**.

Table 1. Binding energy and shift of N 1s and C 1s (C=O) in the polymeric complexes. All core-level spectra were referenced to the C 1s neutral carbon peak at a binding energy (BE) of 285 eV in order to compensate surface charging effects. Shift=BE_C–BE_{4b} (or BE_{5b}), where BE_C, BE_{4b} and BE_{5b} represent the binding energies of the H-bonded complex, acceptor **4b** and donor **5b**, respectively. The binding energy of N 1s is assigned to the nitrogen atom from pyridine, but the binding energy at 400.15 eV corresponding to –N=N– is not listed in the table.

Complexes	N 1s (eV)	Shift (eV)	C 1s (C=O) (eV)	Shift (eV)
4b	399.05	—	—	—
5b	—	—	289.13	—
4b/5a	399.88	0.83	289.00	−0.13
4b/5b	399.97	0.92	288.91	−0.22
4b/5c	399.70	0.65	289.03	−0.10
4a/5b	399.70	0.65	288.96	−0.17
4c/5b	399.83	0.78	288.98	−0.15

acceptor **4b** exhibited two peaks at binding energies of 400.15 and 399.05 eV with an integration of 2:1, being consistent with the fact that the ratio of nitrogen atoms in the azo linkage and in pyridine is 2:1. Therefore, it is deduced that the peak at binding energy of 400.15 eV is attributed to the nitrogen of the azo linkage, while the other peak at 399.05 eV came from the nitrogen of pyridine. In contrast, all of the N 1s spectra of the complexes exhibited only a relatively broad peak at around 400 eV. Upon complexation, the acceptors **4** underwent a larger shift for N 1s (pyridine) but no shift for N 1s (azo) was observed. As a result, the shifted N 1s (pyridine) and intact N 1s (azo) merged as one broad peak.

The shift to a larger binding energy of N 1s (pyridine) in the complexes when compared with uncomplexed species meant that the electron density at the nitrogen of pyridine experienced a net increase. Thus, it can be deduced that the nitrogen of pyridine was involved in the H-bonding interaction, while the nitrogen atoms in the azo linkage were not part of the formation. 'Free', H-bonded and protonated nitrogen lead to different binding energies. Reported results showed that protonated nitrogen demonstrated an increase in binding energy of 2.0 eV or more compared with the 'free' nitrogen atom, while, the binding energy of H-bonded nitrogen increased by less than 1.0 eV (see (*27–32*)). The magnitude of the shifts in binding energy in complexes, **4b/5**, **4a/5b** and **4c/5b**, is in the range of 0.65–0.92 eV and this is indicative of a H-bond association in nature between the acceptor and donor molecules.

In the carbonyl C 1s spectrum of the donor **5b**, a peak emerged at a binding energy of 289.13 eV (Figure 1 (b)). In contrast to the shift of N1s (pyridine) to higher binding energy, the binding energies of carbonyl C 1s for the H-bonded complexes decreased by 0.10–0.22 eV. The formation of the H-bond led to the dissociation of the acid dimer and this, consequently, resulted in the carbonyl oxygen atom not being involved in the H-bond. Therefore, the electron density at the carbonyl carbon atom decreases and thus the binding energy of carbonyl C 1s for the complexes decreased.

In the spectra of **5a** and **6c**, a broad O–H band from 3400 to 2400 cm^{-1} that is typical of an acid dimer was displayed (*33*). However, the FT-IR spectra for the H-bonded complexes demonstrated two new peaks at around 2450 and 1900 cm^{-1} accompanying the disappearance of the broad band from 3400 to 2400 cm^{-1}. The loss of the broad band suggests the absence of the acid dimer in the complexes and that the two new absorption bands are a result of the H-bonding association between the carboxylic acid and pyridine (*34*). In addition, the carbonyl bands (C=O) of the dicarboxylic acid, **5a**, and the mono-substituted carboxylic acid, **6c**, at 1679 and 1681 cm^{-1} respectively, both shifted to higher wavenumbers after complexation as shown in Figure 2. For example, the carbonyl absorption band of the polymeric complexes increased from 1679 to 1690 cm^{-1} and that of the trimeric complexes increased from 1681 to 1692 cm^{-1}. The absorption band at 1690 or 1692 cm^{-1} is attributed to the 'free' carbonyl group of the carboxylic acid whereby the carbonyl oxygen atom did not take part in the formation of H-bond complexes. Likewise, the absorption of pyridine also shifted to larger wavenumbers. For instance, in the polymeric complexes, the absorption band of pyridine increased by 12 cm^{-1} from 1584 to 1596 cm^{-1} (Figure 2 (b)), which is smaller than the increase for pyridine from a 'neutral' state to a protonated state (30 cm^{-1}); see (*30*).

3.3. *DSC and POM study*

The thermal behaviours of the H-bonded complexes were investigated with DSC. The transition temperatures and their associated enthalpy changes for polymeric complexes **4/5** and trimeric complexes **4/6_2** are summarised in Tables 2 and 3, respectively. As examples, the DSC thermograms of the polymeric

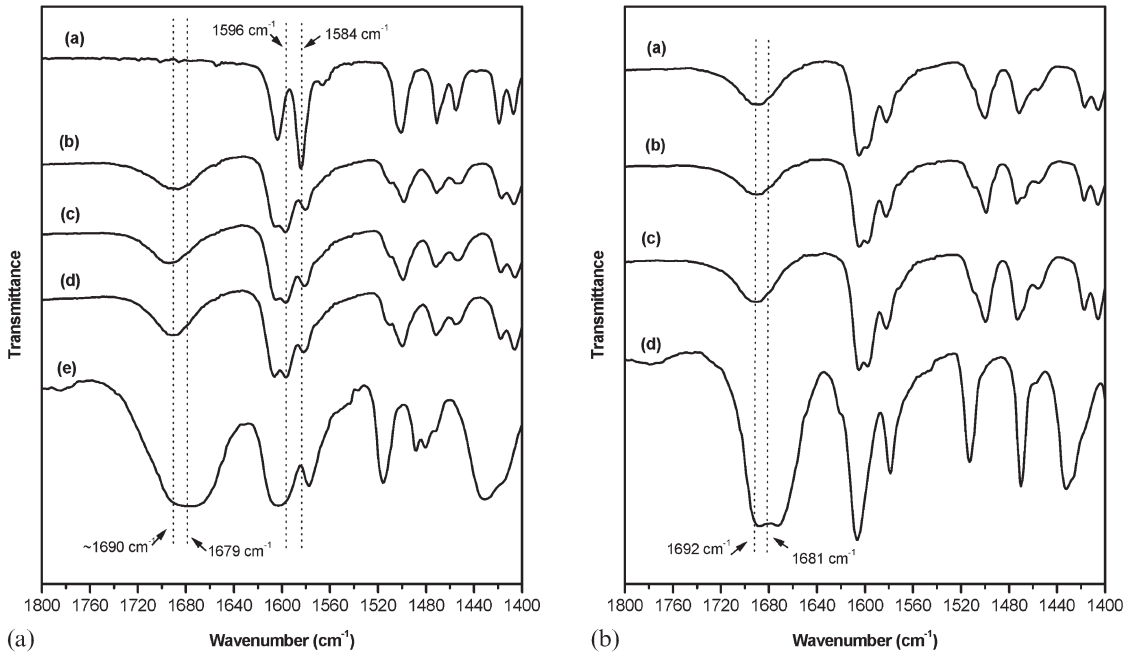

Figure 2. The FT-IR spectra of: (a) polymeric complexes (a) **4c**, (b) **4c/5a**, (c) **4c/5b**, (d) **4c/5c** and (e) **5a** from wavenumbers of 1800 to 1400 cm^{-1}; and (b) trimeric complexes (a) **4a/6c$_2$**, (b) **4b/6c$_2$**, (c) **4c/6c$_2$** and (d) **6c** from wavenumbers of 1800 to 1400 cm^{-1}.

complexes **4b/5** and the trimeric complexes **4a/6$_2$** are illustrated in Figure 3.The pure proton acceptors **4a**–**c** are non-mesogenic and do not exhibit liquid crystalline behaviours as demonstrated by only a sharp phase transition from the crystalline state to the isotropic state upon heating and vice versa on cooling (Figure 3 (a)). However, upon H-bonding association with the proton donors **5a**–**c** and **6a**–**d**, most polymeric and trimeric complexes displayed an entirely different thermal behaviour and more than one phase transition was observed on heating and on cooling, indicating that liquid crystallinity was induced as a result of the complexation. In addition, the complexes could be repeatedly heated and cooled without inducing changes in the phase behaviour, suggesting that the H-bonded LCs are stable.

It is well known that the mesophase transition temperatures for H-bonded liquid crystalline polymers could be controlled by the flexible spacer in the proton acceptors and proton donors. The transition temperatures usually decrease with the increase in length of the flexible spacer between the two mesogenic cores. Figure 4 presents the relationship

Table 2. Thermal behaviour of polymeric complexes **4/5**. Transition temperatures (°C) are taken from the second run. Enthalpies of transition (kJ mol^{-1}) are given in parentheses. Cr, crystalline; N, nematic; I, isotropic.

	Phase transition temperature (°C)	
Complexes	Heating	Cooling
4a/5a	Cr213(93)I	Cr204(88)I
4a/5b	Cr166(61)N186(16)I	$Cr_1$139(38)$Cr_2$152(14)N184(18)I
4a/5c	Cr185(89)I	Cr167(68)N174(17)I
4b/5a	Cr205(97)I	Cr196(85)I
4b/5b	Cr171(49)N181(14)I	Cr162(43)N179(18)I
4b/5c	Cr164(64)N167(18)I	Cr144(63)N165(15)I
4c/5a	Cr210(39)I	$Cr_1$149(18)$Cr_2$179(33)N187(18)I
4c/5b	Cr175(69)I	Cr163(44)N170(16)I
4c/5c	Cr154(30)N159(54)I	Cr144(60)N158(16)I

Table 3. Thermal behaviour of complexes **4/6$_2$**. Transition temperatures (°C) are taken from the second run. Enthalpies of transition (kJ mol^{-1}) are given in parentheses. Cr, crystalline; N, nematic; I, isotropic.

	Phase transition temperature (°C)	
Complexes	Heating	Cooling
4a/6a$_2$	Cr169(85)N177(11)I	Cr157(87)N173(13)I
4a/6b$_2$	Cr157(78)N170(13)I	Cr150(70)N168(14)I
4a/6c$_2$	Cr150(70)N166(14)I	Cr144(71)N163(14)I
4a/6d$_2$	Cr150(76)N162(15)I	Cr144(77)N160(15)I
4b/6a$_2$	Cr168(103)N170(8)I*	Cr157(82)N166(13)I
4b/6b$_2$	Cr147(83)N163(13)I	Cr139(80)N161(15)I
4b/6c$_2$	Cr143(83)N159(13)I	$Cr_2$131(31)$Cr_1$135(39) N156(13)I
4b/6d$_2$	Cr139(78)N155(13)I	Cr133(78)N153(14)I
4c/6a$_2$	Cr139(55)N159(13)I	Cr126(64)N157(14)I
4c/6b$_2$	Cr152(89)N(11)I*	Cr135(60)N152(13)I
4c/6c$_2$	Cr140(76)N150(11)I	Cr128(77)N148(13)I
4c/6d$_2$	Cr137(68)N146(11)I	Cr130(72)N144(13)I

*Enthalpies of transition (N–I) were estimated by DSC when a heating rate of 1°C min^{-1} was applied.

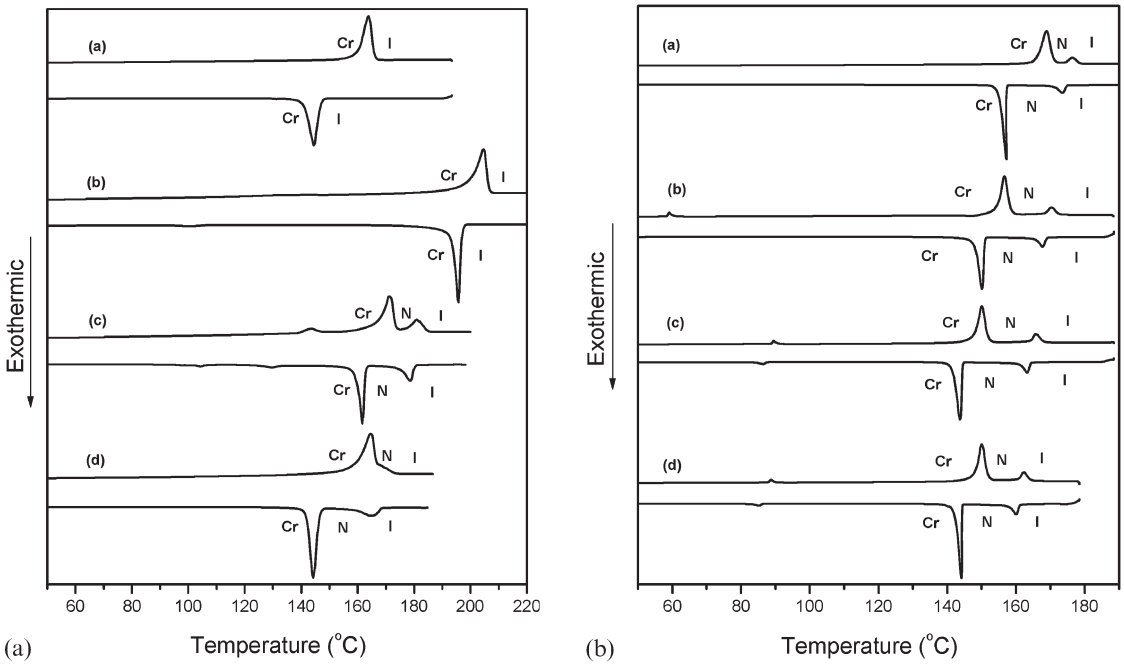

Figure 3. The DSC thermograms of: (a) polymeric complexes (a) **4b**, (b) **4b/5a**, (c) **4b/5b** and (d) **4b/5c**; and (b) trimeric complexes (a) **4a/6a$_2$**, (b) **4a/6b$_2$**, (c) **4a/6c$_2$** and (d) **4a/6d$_2$**.

between isotropic to nematic phase transition temperatures ($T_{I–N}$) of complexes **4/5** and **4/6$_2$** as well as reported complexes **7/5** (see (*11*)) and the length of the spacer in the proton acceptors and donors. The transition temperatures $T_{I–N}$ for polymeric complexes decreases as the spacer length in the proton donors **5** increases as shown in figure 4 (a). For instance, $T_{I–N}$ of **4c/5** complexes showed a drop of 29°C from 187 to 158°C as the number of oxyethylene units in the proton donors increases from 3 to 5. Similarly, the $T_{I–N}$ also decrease as the spacer length in the proton acceptors **4** increases. For instance, the $T_{I–N}$ of complexes **4/5c** decreases from 174 to 158°C as the number of methylene units in **4** increases from 8 to 12. With comparison to reference complexes **7/5**, complexes **4/5** show relatively lower $T_{I–N}$ than the corresponding complexes **7/5**. This is because the azopyridine unit is more flexible than the stilbazolyl unit. The isomerisation energy barrier for azo from *trans* to *cis* is 100 kJ mol^{-1}, which is much lower than that for the C=C bond (150 kJ mol^{-1}); see (*35, 36*).

Likewise, the $T_{I–N}$ for the trimeric polymeric complexes showed a consistent decrease as the spacer length in the proton acceptors **4** or the length of the terminal group in the proton donors **6** increases. As an example, a drop from 157 to 144°C was observed in the $T_{I–N}$ of **4c/6$_2$** complexes when the number of methylene units in the terminal group increase from 6

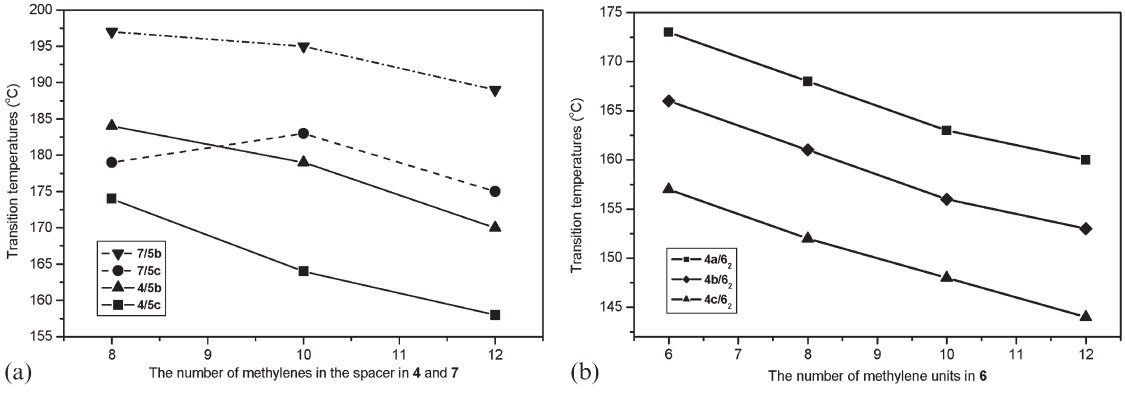

Figure 4. The transition temperatures $T_{I–N}$ of complexes plotted against the length of spacer in the proton acceptor. (a) The polymeric complexes **4/5** and **7/5** on cooling ($T_{I–S}$ of complexes **7/5** are taken from (*11*)); and (b) trimeric complexes **4/6$_2$** on cooling.

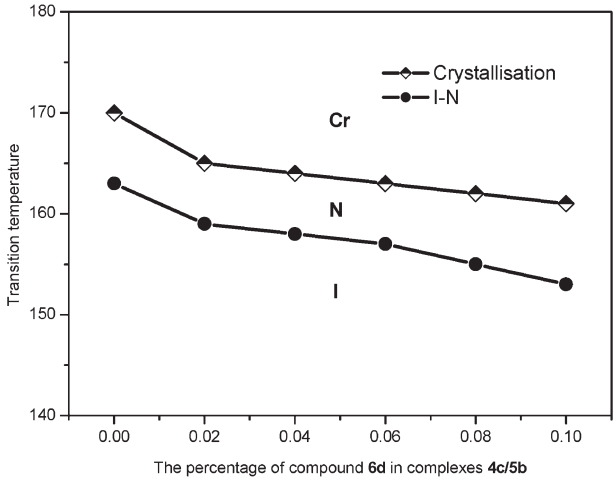

Figure 5. The phase transition temperatures of complexes **4c/5b** against the composition of monofunctional proton donor **6d**. (Complex composition: $\mathbf{4c_{0.5}/5b}_x\mathbf{/6d}_y$, $x+y=0.5$, $y=0$–0.1.)

to 12. Similarly, the $T_{I–N}$ of $\mathbf{4/6d_2}$ declined from 160 to 144°C as the spacer length increased from 8 methylene units to 12. The above results demonstrate that the length of the spacer in the proton donor and acceptor molecules has a critical effect on the thermal behaviours of the H-bonded main-chain azo-containing complexes. Thus, the length in the spacer can be easily exploited as an element to tune the phase transition temperatures of the complexes.

A question may arise as to the degree of polymerisation for linear H-bonded supramolecular systems. It was reported that a non-liquid crystalline system at room temperature has a degree of polymerisation of 12–15 (see (*37*)). The effect of different ratios of two difunctional monomers AA and BB on the phase transition temperatures was studied by Alexander et al. (*38*). The results showed that the maximum mesomorphic transition temperatures were observed at 1:1 stoichiometry, suggesting that at the 1:1 composition for two monomers, the maximum degree of polymerisation was achieved. The studies (*39*) on the H-bonded complexes also showed that fibres could be drawn from such complexes at their nematic phase, which is very similar to conventional covalent bond polymers. The X-ray fibre scattering pattern of the complexes indicated that the complexes were oriented under shear force of drawing. The composition effects by adding a small amount of a monofunctional proton donor molecule **6d** to complex **4c/5b** were investigated. Figure 5 shows the phase transition temperatures against the composition of **6d**. It was clear that the crystallisation and I–N phase transition temperatures constantly shifted to lower values as the composition of **6d** increases. This is likely because more polymeric chains become shorter owing to the capping of **6d**. The result is in fact in agreement with the previous study (*38*) where the complex at 1:1 stoichiometry has the maximum mesomorphic transition temperatures and hence the longest polymeric chain. At the same time the associated enthalpy for each I–N phase transition decreased from 16 to 13 kJ mol^{-1} as the composition of **6d** increased from 0 to 0.1. Similarly, trimeric complexes $\mathbf{4/6_2}$ showed a relatively lower enthalpy than those polymeric complexes, implying that the addition of a monofunctional component would reduce the degree of polymerisation. This is consistent with the reported result that a polymeric complex has higher enthalpy change than an oligomeric complex (*37*).

The phase identification of the H-bonded LCs was studied using POM. Complexes of **4/5** and $\mathbf{4/6_2}$ developed the schlieren, threaded and droplet textures that are typical for nematic phase. The selected textures for polymeric complexes are shown in Figure 6. All trimeric complexes exhibited enantropic

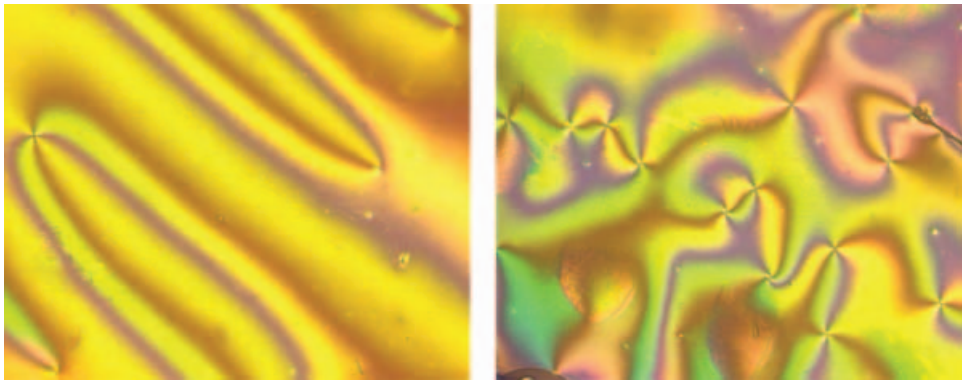

(a) (b)

Figure 6. The polarising optical micrographs of polymeric complexes: (a) **4a/5b** at 183°C, nematic, on heating; (b) **4b/5b** at 174°C, nematic, on cooling.

LCs; however, some polymeric complexes, for example **4a/5a**, **4a/5c**, **4b/5a**, **4c/5a** and **4c/5b**, displayed only monotropic LCs. Unlike the analogous stilbazole-based complexes **7/5**, only nematic phases for the azo-containing complexes were observed, suggesting that the azo mesogenic core in these systems tends to form a less-ordered LC phase because of the lower rigidity in the mesogenic core.

3.4. *Study of the UV–vis spectra of the complexes*

The photoactivities of the hydrogen-bonded main-chain azopyridine polymers were investigated using UV–visible spectroscopy. Figure 7 shows the UV–vis spectra of complex **4a/5b** before and after UV irradiation in the film state. In general, upon UV irradiation at around 360 nm, the energetically more stable elongated *trans* configuration of the azo molecule changes into a bent *cis* configuration. This is demonstrated by a decrease in the intensity of the π–π^* absorption band at 355 nm of the *trans*-isomer and an increase in the n–π^* band absorption at 450 nm of the *cis*-isomer (*26*). The reverse transformation can take place by illumination with visible light in the range of 400–500 nm (see (*40*)). Indeed, in most studied cases of side-chain azopyridine polymers, *trans-cis* transformation and vice versa are very common and are easily attained (*22*).

In contrast to side-chain azopyridine polymers, the H-bonded main-chain azopyridine polymers, however, were not remarkably responsive to the light. For complexes **4a/5b**, a small decrease in intensity of absorption corresponding to the π–π^* absorption band of the azo group at around 360 nm in the UV–vis spectra was observed upon UV irradiation at 365 nm (0–300 s), but a negligible change at around 450 nm was detected. In complex **4a/5b**, the proton acceptor **4a** is locked by two dibenzoic acids via the two hydrogen bonds as illustrated in Figure 8. As a result, the pseudopolymer chain became less flexible owing to conformational constraints caused by the hydrogen bonds and the polymer main chain. It is speculated that *trans–cis* photoisomerisation is therefore inhibited significantly. In contrast, in side-chain polymeric complexes, the azopyridine compound is fixed only at one end by the hydrogen bond and thus more flexible. In addition, earlier studies of side-chain azopyridine polymers had shown that benzoic acid complexes with azopyridine exhibited less light-sensitive responsive properties than aliphatic acid complexes (*22*).

4. Conclusions

In this paper, we have reported on the synthesis of main-chain H-bonded azo-containing liquid crystalline polymeric and trimeric complexes. Most of the azo-containing complexes exhibited nematic phases over a relatively wide range of 20–30°C. By comparing these complexes with the similar stilbazolyl derivatives, the formation of the only less-ordered nematic phase and relatively lower phase transition temperatures are probably a result of the lower rigidity of azo linkage. The length effects of the spacer in the proton donors and acceptors on phase transition temperatures have been investigated, revealing that an increase in length of the spacer in the proton donors or proton acceptors resulted in a

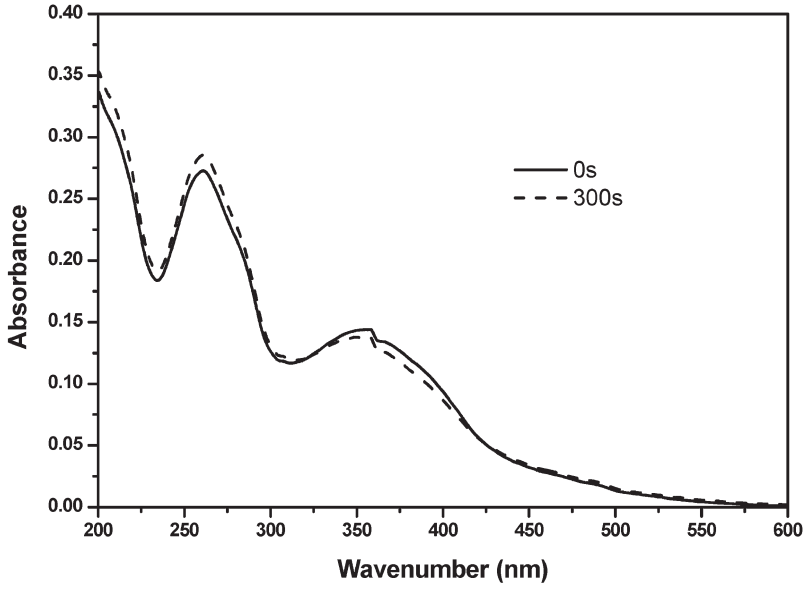

Figure 7. The UV–visible spectra of **4a/5b**.

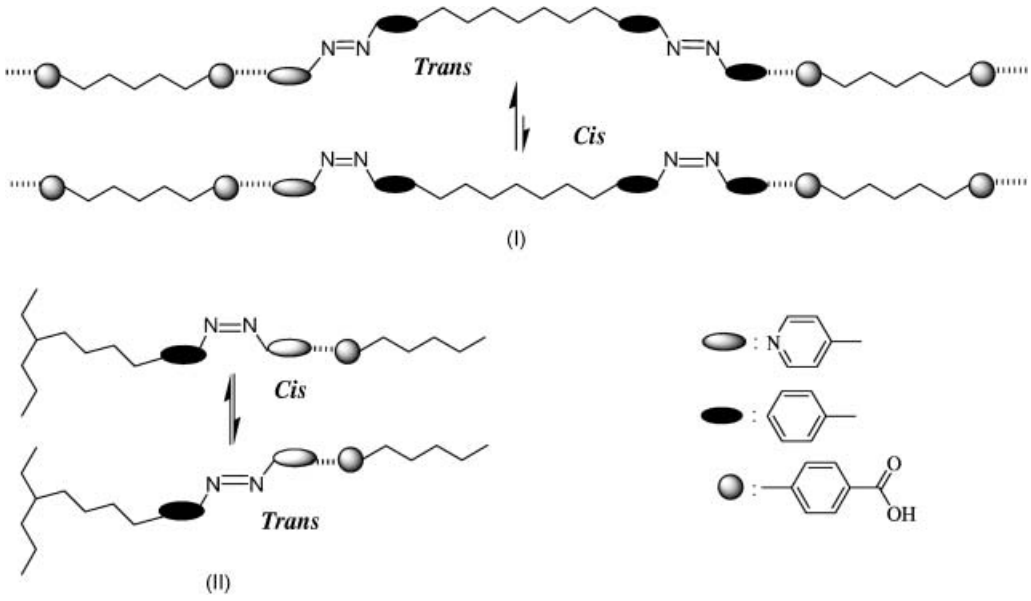

Figure 8. Azo-containing (I) main-chain and (II) side-chain H-bonded polymers.

decrease in the transition temperatures. The preliminary study on photoactivity of the azo-containing polymeric complexes in a film state shows that the photoisomerisation is significantly suppressed probably as a result of less freedom in the conformational changes.

Acknowledgement

Financial support for this work was provided by the Institute of Materials Research and Engineering (IMRE).

References

(1) Paleos C.M.; Tsiourvas D. *Angew. Chem. Int. Ed. Engl.* **1995**, *34*, 1696–1711.
(2) Kato T. *Handbook of Liquid Crystals*; Demus D., Gray G.W., Goodby J., Spiess H.-W., Vill V. (Eds), Wiley-VCH: Weinheim, 1998.
(3) Kihara H.; Kato T. *Macromol. Rapid Commun.* **1997**, *18*, 281–286.
(4) Bladon P.; Griffin A.C. *Macromolecules* **1993**, *26*, 6604–6610.
(5) Lee C.M.; Jariwala C.P.; Griffin A.C. *Polymer* **1994**, *35*, 4550–4554.
(6) Pourcain C.B.S.; Griffin A.C. *Macromolecules* **1995**, *28*, 4116–4121.
(7) Lee C.M.; Griffin A.C. *Macromol. Symp.* **1997**, *117*, 281–290.
(8) He C.; Donald A.M.; Griffin A.C.; Waigh T.; Windle A.H. *J. Polym. Sci. Part B: Polym. Phys.* **1998**, *36*, 1617–1624.
(9) Lee M.; Cho B.K.; Kang Y.S.; Zin W.C. *Macromolecules* **1999**, *32*, 8531–8537.
(10) Lehn J.M. *Adv. Mater.* **1990**, *2*, 254–257.
(11) Lehn J.M. *Chem. Commun.* **1994**, 197–199.
(12) Toh C.L.; Xu J.; Lu X.; He C. *J. Polym. Sci. Part A: Polym. Chem.* **2005**, *43*, 4731–4743.
(13) Xu J.; Toh C.L.; Liu X.; Wang S.; He C.; Lu X. *Macromolecules* **2005**, *38*, 1684–1690.
(14) Ichimura K. *Chem. Rev.* **2000**, *100*, 1847–1873.
(15) Ikeda T. *J. Mater. Chem.* **2003**, *13*, 2037–2057.
(16) Ikeda T.; Wu Y. *Pure Appl. Chem.* **1999**, *71*, 2131–2136.
(17) Eich M.; Wendorff J.H.; Reck B.; Ringsdorf H. *Makromol. Chem. Rapid Commun.* **1987**, *8*, 59–63.
(18) Eich M.; Wendorff J.H. *Makromol. Chem. Rapid Commun.* **1987**, *8*, 467–471.
(19) Anderle K.; Birenheide R.; Werner M.J.A.; Wendorff J.H. *Liq. Cryst.* **1991**, *9*, 691–699.
(20) Kato T.; Mizoshita N.; Kishimoto K. *Angew. Chem. Int. Ed.* **2006**, *45*, 38–68.
(21) Ikeda T.; Mamiya J.-I.; Yu Y. *Angew. Chem. Int. Ed.* **2007**, *46*, 506–528.
(22) Li C.; Zhao Y. *Chem. Mater.* **2004**, *16*, 2076–2082.
(23) Zhao Y. *Pure Appl. Chem.* **2004**, *76*, 1499–1508.
(24) Mallia V.A.; Antharjanam P.K.S.; Das S. *Liq. Cryst.* **2003**, *30*, 135–141.
(25) Aoki K.; Nakagawa M.; Ichimura K. *J. Am. Chem. Soc.* **2000**, *122*, 10,997–11,004.
(26) Antharjanam P.K.S.; Mjay V.A.; Das S. *Chem. Mater.* **2002**, *14*, 2687–2692.
(27) Xu J.; He C.; Toh K.C.; Lu X. *Macromolecules* **2002**, *35*, 8846–8851.
(28) Luo X.F.; Goh S.H.; Lee S.Y.; Huan C. *Macromol. Chem. Phys.* **1999**, *200*, 874–880.
(29) Goh S.H.; Lee S.Y.; Dai J.; Tan K.L. *Polymer* **1996**, *37*, 5305–5308.
(30) Zhou X.; Goh S.H.; Lee S.Y.; Tan K.L. *Appl. Surf. Sci.* **1998**, *126*, 141–147.
(31) Zhou X.; Goh S.H.; Lee S.Y.; Tan K.L. *Polymer* **1998**, *39*, 3631–3640.
(32) Luo X.F.; Goh S.H.; Lee S.Y.; Tan K.L. *Macromolecules* **1998**, *31*, 3251–3254.

(33) Lee J.Y.; Painter P.C.; Coleman M.M. *Macromolecules* **1980**, *21*, 346–354.
(34) Kumar U.; Kato T.; Uryu T.; Frechet J.M.J. *J. Am. Chem. Soc.* **1992**, *114*, 6630–6639.
(35) Talaty E.R.; Fargo J.C. *Chem. Commun.* **1967**, 65–66.
(36) Yamashita S.; Ono H.; Toyama O. *Bull. Chem. Soc. Jpn.* **1962**, *35*, 1849–1853.
(37) Hilger C.; Stadler R. *Makromol. Chem.* **1991**, *192*, 805–817.
(38) Alexander C.; Jariwala C.P.; Lee C.M.; Griffin A.C. *Macromol. Symp.* **1994**, *77*, 283–294.
(39) Lu X.; He C.; Terrell C.D.; Griffin A.C. *Macromol. Chem. Phys.* **2002**, *203*, 85–88.
(40) Prasad S.K.; Geetha G.N.; Sandhya K.L.; Rao D.S.S. *Curr. Sci.* **2004**, *86*, 815–823.